ChemComm

COMMUNICATION

Cite this: *Chem. Commun.*, 2024, **60**, 2800

Received 21st December 2023,
Accepted 11th February 2024

DOI: 10.1039/d3cc06212k

rsc.li/chemcomm

Dual space divergence in small molecule quasiracemates: benzoyl leucine and phenylalanine assemblies†

Katelyn N. Koch, Aaron J. Teo and Kraig A. Wheeler *

Quasiracemic materials constructed with two points of structural difference were used to understand the role molecular shape plays in molecular assembly. Hot stage, crystallographic and occupied cavity space assessments provide insight into how imposed CH_3/Cl and H/CF_3 structural variations placed on benzoyl leucine and phenylalanine scaffolds result in a remarkably high occurrence of cocrystal formation.

Quasiracemic materials represent a broad class of compounds created by the pairing of near enantiomers.[1,2] Because these materials exploit the molecular shape and chirality of the quasienantiomeric components in supramolecular assembly, it is not surprising that this approach has successfully been applied to construct material architectures that require precise control over the alignment of the building blocks.[3–16] Similar to the concepts of polymorphism[17] and crystal structure prediction,[18–20] the phenomenon of quasiracemate formation is straightforward and direct in principle. However, a considerable challenge exists in defining the structural boundaries and shape space of the assembled materials. The challenge arises in the design stage, where the inherent flexibility of the term quasiracemate – equimolar ratios of chemically unique compounds of opposite handedness – intentionally lacks details of the chemical frameworks, functional groups and structural difference limitations needed for successful quasiracemate formation. Literature reports suggest that the structural variation between small molecule quasienantiomers occurs at only one site with a relatively minor imposed structural difference – *e.g.*, Cl/Br[21–25] and CH_3/Cl[21,23,26] represent common pairings. Though this strategy continues to show success with quasiracemate assembly, it also presents questions relating to a broader understanding of the term quasiracemate and the degree of structural tolerance permitted during quasiracemate assembly.

To investigate the structural boundaries of molecular shape-directed molecular recognition, the present work aims to develop a new approach that targets quasiracemic scaffolds designed with two points of chemical difference. We chose to combine benzoyl leucine (**1**) and phenylalanine (**2**) quasienantiomers, where the imposed topological variation of these components can be estimated by the percent difference in the R group volumes (%ΔV = 18.0). Drawing from previous quasiracemate successes and a list of common functional groups (Fig. 1), the leucine and phenylalanine systems include additional functionalization using the CH_3/Cl (%ΔV = 4.0) and H/CF_3 (%ΔV = 138.7) substituent pairs. While CH_3/Cl[21,23,26] are familiar group selections with only modest size and shape space differences, the H/CF_3 combination is absent in small molecule quasiracemates, likely owing to their considerable topological differences. The design element using two sites of chemical difference provides an opportunity to examine sizable families of ten cocrystalline materials that differ iteratively in their shape space and pendant functional groups X and X′, where X/X′ represents the CH_3/Cl and H/CF_3 pairings. The ten unique CH_3/Cl and H/CF_3 compounds consist of racemates [(±)-**1**-X, (±)-**1**-X′, (±)-**2**-X, (±)-**2**-X′], singly different quasiracemates [**1**-X/**1**-X′, **2**-X/**2**-X′, **1**-X/**2**-X, **1**-X′/**2**-X′] and doubly distinct quasiracemates [**1**-X/**2**-X′, **1**-X′/**2**-X]. By examining the

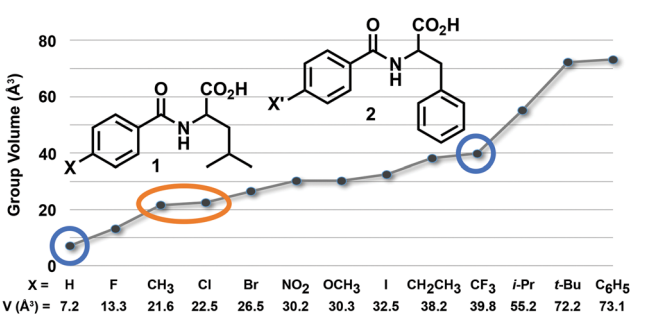

Fig. 1 Chemical architectures of benzoyl leucine **1** and phenylalanine **2** showing common functional groups and their group volumes.

Department of Chemistry, Whitworth University, 300 West Hawthorne Road, Spokane, Washington, 99251, USA. E-mail: kraigwheeler@whitworth.edu

† Electronic supplementary information (ESI) available. CCDC 2312799–2312815. For ESI and crystallographic data in CIF or other electronic format see DOI: https://doi.org/10.1039/d3cc06212k

cocrystallization behavior using melt and solvent-assisted methods, this work seeks a deeper understanding of the role of molecular topology in molecular assembly.

Hot stage thermomicroscopy. Video assisted hot stage microscopy offers a useful diagnostic tool for the present study by probing crystal nucleation from the melt.[27–30] For racemates and quasiracemates, the thermal signature from heating the two components produces a virtual melting point phase diagram showing either conglomerate formation or the growth of a new crystalline phase at the component interface. Fig. 2 depicts this process with the (±)-**1**-CF_3 and L-**1**-CF_3/D-**2**-H systems, where the thermal micrographs show the emergence of two eutectic regions and a racemic or quasiracemic phase with increasing temperature.

Processing all possible CH_3/Cl and H/CF_3 enantiomeric and quasienantiomeric sets of the components *via* the hot stage method offers insight into how systematic changes in molecular topology affect molecular recognition. Fig. 3 shows these results and the %Δ*V* values‡ for each system. When considering the leucine **1** and phenylalanine **2** enantiomers combined with the H, CH_3, Cl and CF_3 substituents, all but (±)-**1**-H showed racemate formation. In this case, the lack of success in bringing together the L and D components highlights the inherent limitation of the hot stage method for materials that decompose at elevated temperatures.

For the quasiracemates, the hot stage successes correlate well with the %Δ*V* values. The six CH_3/Cl systems vary from %Δ*V* = 0.8 to 15.0% with each forming cocrystalline materials. Combining the H/CF_3 quasienantiomers (%Δ*V* = 12.0–45.8) tells a different story, where four of these systems result in quasiracemates (*i.e.*, **1**-H/**2**-H, **2**-H/**1**-CF_3, **2**-H/**2**-CF_3, **1**-CF_3/**2**-CF_3). The remaining **1**-H/**1**-CF_3 and **1**-H/**2**-CF_3 compounds exhibit the most significant %Δ*V* range (34.3 and 45.8%, respectively) and do not achieve quasiracemic crystals from the melt.

Crystallography. Given the range of chemical variation for the CH_3/Cl system, it is somewhat surprising that each of the ten targeted compounds gave suitable samples for crystallographic assessment (Table S1, ESI†). These structures lack disorder and

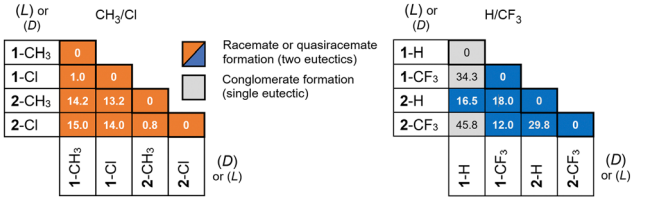

Fig. 3 Results from hot stage thermomicroscopy for the racemates and quasiracemates of **1** and **2** with the CH_3/Cl and H/CF_3 substituent pairs. The percent difference in volumes (%Δ*V*) is also provided for each system.

align components in one of two crystalline phases. The majority crystallize into Form I with either space group $P2_1/c$ (racemates) or $P2_1$ (quasiracemates) and display similar unit cell parameters, crystal packing and $R_2^2(10)$ N–H···O=$C_{carboxyl}$ and $C(7)$ (O–H···O=C_{amide}) hydrogen-bond motifs[31,32] (Fig. 4a and Table S2, ESI†). Many of these structures that take on Form I also exhibit close π–π stacking of the benzoyl groups (Table S3, ESI†). Interestingly, those structures constructed from only leucine **1** components [*i.e.*, (±)-**1**-CH_3, (±)-**1**-Cl and D-**1**-CH_3/L-**1**-Cl] assemble differently *via* Form II (space groups $P2_1/c$ and $P2_1$) with $R_2^2(8)$ carboxylic acid O–H···O=C hydrogen-bonded dimers and N–H···O=C_{amide} $C(4)$ interactions (Fig. 4b). The $R_2^2(10)$ (Form I) and $R_2^2(8)$ (Form II) motifs are positioned on inversion symmetry elements for the racemates and approximate inversion relationships for the quasiracemic systems.

Similar to the hot stage experiments, crystal growth of the H/CF_3 family proved challenging compared to the CH_3/Cl system. Three racemates [(±)-**1**-H, (±)-**1**-CF_3, (±)-**2**-H] and four quasiracemates [D-**2**-H/L-**2**-CF_3, L-**1**-H/D-**2**-H, L-**1**-CF_3/D-**2**-CF_3, D-**1**-CF_3/L-**2**-H]) gave suitable crystals for structure determination with an increased occurrence of Form I [(±)-**1**-H, (±)-**2**-H, D-**2**-H/L-**2**-CF_3, L-**1**-H/D-**2**-H, L-**1**-CF_3/D-**2**-H] relative to Form II [(±)-**1**-CF_3]. The structure of L-**1**-CF_3/D-**2**-CF_3 displays a third crystalline phase that exhibits matching hydrogen-bond contacts to Form I but deviates in molecular alignment resulting from F···F or F···H interactions. Crystal growth experiments involving (±)-**2**-CF_3 and

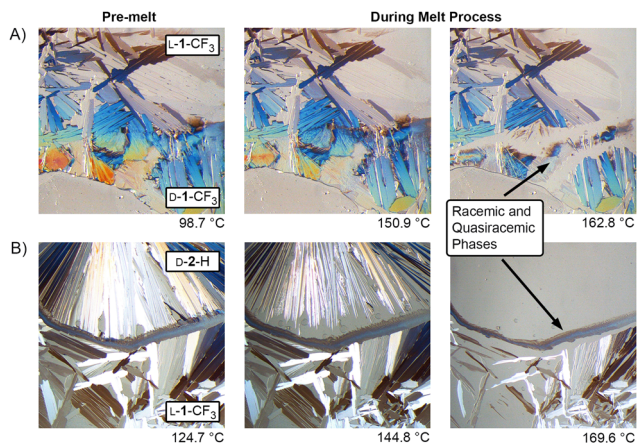

Fig. 2 Hot stage thermomicroscopy micrographs of (A) L-**1**-CF_3/D-**1**-CF_3 and (B) L-**1**-CF_3/D-**2**-H.

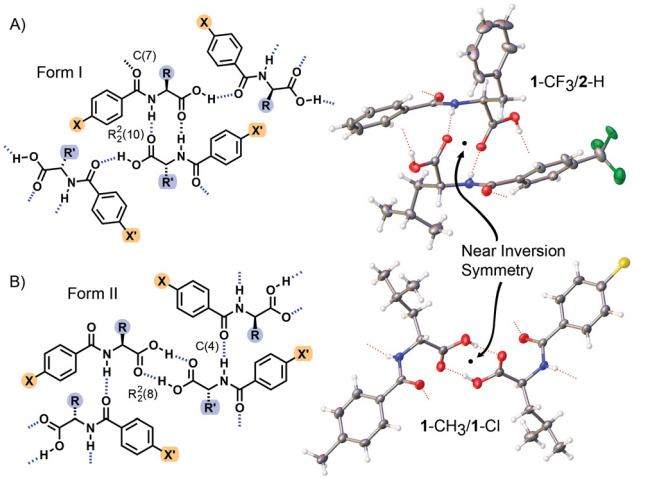

Fig. 4 Depictions of the hydrogen-bond motifs (Form I and II) and the crystal structures of quasiracemates D-**1**-CF_3/L-**2**-H and D-**1**-CH_3\L-**1**-Cl.

quasiracemates **1**-H/**1**-CF_3 and **1**-H/**2**-CF_3 did not produce suitable samples for crystallographic assessment even after multiple attempts using various solvent systems and methods.

The extent of isomorphism observed within Form I and II was further studied and confirmed using the Crystal Structure Similarity search feature in CCDC-Mercury (v2022.3.0, ref. 33) (Table S4, ESI†). This assessment method quantitatively measures the crystal packing likeness for pairs of structures that, when applied to systems **1** and **2**, showed the expected trends with distinctions related to Leu/Phe, CH_3/Cl, and H/CF_3 structural differences. In view of the structural similarity of the components and their propensity to align with one of two primary motifs, the likelihood of polymorphism should be high. While it is possible Form I and II represent two potential polymorphic phases, this study did not encounter polymorphism.

Another important structural feature of the H/CF_3 system is the presence of disorder in the leucine [(±)-**1**-CF_3, L-**1**-H/D-**2**-H and D-**1**-CF_3/L-**2**-H] and CF_3 [L-**1**-CF_3/D-**2**-CF_3 and D-**1**-CF_3/L-**2**-H] groups. While CF_3 disorder is pervasive in the crystal structures of aryl CF_3 groups (Cambridge Crystallographic Database, v5.43, ref. 34), where 42% of the deposited 5804 structures were modeled with disorder, only 10% of the leucinyl entries contain disorder. The observation of disorder in several of our structures is potentially significant when considering how the imposed topological difference of the leucine **1** and phenylalanine **2** quasienantiomeric components (%$\Delta V_{\text{Leu–Phe}}$ = 18.0%) are accommodated during the molecular assembly process.

Lattice energy calculations using Crystal Explorer[35] (Gaussian,[36] B3LYP/6-31g(d,p)) and differential scanning calorimetry (DSC) give details on the crystal energetics of these systems. Collectively, the structures constructed solely from phenylalanine **2** achieve ~20 kJ mol^{-1} greater stability than those restricted to the leucine **1** framework (Table S5, ESI†). Even so, the lattice energy (E_{Latt}) calculations for the quasiracemates are, in many cases, comparable regardless of component selection. An E_{Latt} of −177 kJ mol^{-1} (E_{Latt}(DSC) = −68 kJ mol^{-1}) for quasiracemate **1**-Cl/**2**-CH_3 and that for (±)-**1**-Cl and (±)-**2**-CH_3 are −164 kJ mol^{-1} (E_{Latt}(DSC) = −65 kJ mol^{-1}) and −190 kJ mol^{-1} (E_{Latt}(DSC) = −91 kJ mol^{-1}), respectively. This trend in E_{Latt} values suggests that the observed structural mimicry of inversion symmetry in the quasiracemates results from the favorable close alignment achieved in the racemate examples.

Occupied cavity spaces. Void space determinations reveal the crystal packing efficiencies of the leucine (Leu) and phenylalanine (Phe) side chains. Given the isomorphic nature of many of these structures and that the Leu and Phe R groups differ significantly in size and shape (%ΔV of 18%), we questioned how the crystal assemblies of these systems can accommodate quasienantiomeric components with drastically different shape spaces. Fig. 5a shows the result obtained using CCDC-Mercury to determine the cavity space occupied by the Leu (261.6 Å^3) and Phe (308.9 Å^3) R groups of quasiracemate **1**-CH_3/**2**-Cl. Applying Kitaigorodskii's packing coefficient (C_p) approach[37,38] to cavity spaces allows a direct comparison of these crystallographic voids to the literature volumes of the Leu ($V_{CH_2(CH_3)_2}$ = 71.6 Å^3) and Phe ($V_{CH_2C_6H_5}$ = 85.8 Å^3) groups,[39] where $C_p = V_{\text{group}}/V_{\text{cavity}}$ (Table S6, ESI†). In the case of **1**-CH_3/**2**-Cl, the C_p(Leu) and C_p(Phe) values

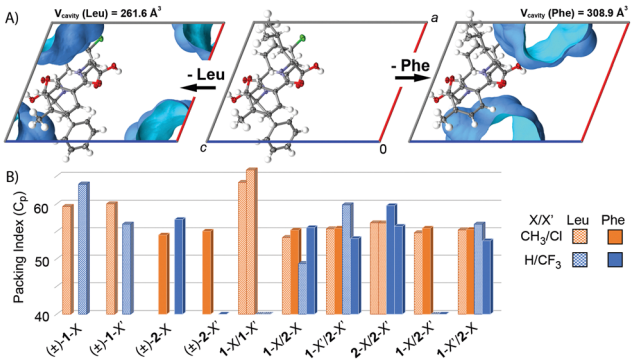

Fig. 5 Leu and Phe (A) cavity spaces for quasiracemate D-**1**-CH_3/L-**2**-Cl using a 1.4 Å probe radius 0.1 Å grid spacing and (B) packing coefficients for the CH_3/Cl and H/CF_3 systems.

for the two components are 0.55 and 0.56, respectively, indicating comparable packing efficiencies for these different amino acid side chains. From inspection of the entire CH_3/Cl system, the structures with at least one phenylalanine **2** component align the Leu side chains with C_p values ranging from 0.54 to 0.55 (Fig. 5B); whereas crystals composed of only leucine **1** (*i.e.*, (±)-**1**-CH_3, (±)-**1**-Cl and **1**-CH_3/**1**-Cl) pack more efficiently (C_p = 0.60–0.66). This result seems counterintuitive since sterically encumbered groups such as the leucine side chain should translate to less effective packing. A similar trend in C_p values is observed for the H/CF_3 system with the exception of (±)-**1**-CF_3, **1**-H/**2**-H and **1**-CF_3/**2**-H structures. In those cases, the %ΔV values are less (0.49–0.56) and indicate additional space required to accommodate the disordered Leu groups.

When considering all CH_3/Cl and H/CF_3 quasiracemic structures containing both Leu and Phe and excluding those with disorder, the packing efficiencies of the Leu (C_p(ave) = 0.56 with a range of 0.54–0.60) and Phe (C_p(ave) = 0.55, 0.54–0.56) groups are remarkably similar. Outside of the leucine dominant **1**-CH_3/**1**-Cl quasiracemate (C_p = 0.64 and 0.66), the use of Form I or II does not meaningfully affect packing efficiencies. When paired with phenylalanine **2** components, these results show that the cavity occupied by the Leu group is larger, with packing efficiencies similar to Phe. This similarity effectively creates crystal architectures that more closely mimic the spatial distribution of the enantiomers found in the racemates of **1** and **2**.

We have described a fundamentally different approach to creating quasiracemic materials. Most previous approaches pair quasienantiomeric components where the structural difference is limited to one site and sterically similar groups.

By cocystallizing the benzoyl leucine **1** and phenylalanine **2** quasienantiomeric components *via* robust hydrogen-bond motifs, these systems are able to accommodate additional CH_3/Cl and H/CF_3 substitutions and large spatial differences between the quasiracemic components. Hot stage thermomicroscopy and crystallographic approaches reveal the structural boundaries for these systems and the structural preference for near-inversion symmetry. Void space determinations of the Leu and Phe side groups for the quasiracemates indicate that smaller leucine component **1** takes up a larger space than anticipated to accommodate quasiracemate formation.

Conceptualization, K. A. W.; methodology, K. A. W.; formal analysis, K. N. K., A. J. T. and K. A. W.; funding acquisition, K. A. W.; investigation, K. N. K., A. J. T. and K. A. W.; supervision, K. A. W.; project administration, K. A. W.; validation, K. N. K., A. J. T. and K. A. W.; visualization, K. N. K., A. J. T. and K. A. W.; writing – original draft, K. A. W.; writing – review and editing, K. N. K., A. J. T. and K. A. W. All authors have read and agreed to the published version of the manuscript.

We gratefully acknowledge financial support from the National Science Foundation (DMR2304042 and CHE1827313). We also thank Prof. B. Foxman (Brandeis Univ.) for review of the manuscript and helpful discussions.

Conflicts of interest

There are no conflicts to declare.

Notes and references

‡ The percent difference in volume (%ΔV) was determined as $[(|V_1 - V_2|/(V_1 + V_2)/2] \times 100)$, where $V_1 = V_X + V_R$ and $V_2 = V_{X'} + V_{R'}$ are the summation of the cavity volumes for the pendant substituents (X and X′) and amino acid side chains (R and R′)

1 A. Fredga, *Bull. Soc. Chim. Fr.*, 1973, **1**, 173–182.
2 Q. Zhang and D. P. Curran, *Chem. – Eur. J.*, 2005, **11**, 4866–4880.
3 M. M. H. Smets, E. Kalkman, A. Krieger, P. Tinnemans, H. Meekes, E. Vlieg and H. M. Cuppen, *IUCrJ*, 2020, **7**, 331–341.
4 U. K. Shrestha, A. E. Golliher, T. D. Newar, F. O. Holguin and W. A. Maio, *J. Org. Chem.*, 2021, **86**, 11086–11099.
5 Q. Ronzon, W. Zhang, T. Charote, N. Casaretto, G. Frison and B. Nay, *Angew. Chem., Int. Ed.*, 2024, **61**, e202212855.
6 D. F. Bánhegyi, E. Fogassy, J. Madarász and E. Pálovics, *Molecules*, 2022, **27**, 3134.
7 D. F. Bánhegyi, E. Fogassy and E. Pálovics, *Symmetry*, 2021, **13**, 1516.
8 T. Nakakoji, H. Sato, D. Ono, H. Miyake, E. Mieda, S. Shinoda, H. Tsukube, H. Kawasaki, R. Arakawa and M. Shizuma, *RSC Adv.*, 2021, **11**, 36237–36241.
9 T. Nakakoji, H. Sato, D. Ono, H. Miyake, S. Shinoda, H. Tsukube, H. Kawasaki, R. Arakawa and M. Shizuma, *Chem. Commun.*, 2020, **56**, 54–57.
10 L. Lodhi, J. P. Yadav, T. Yamazaki, N. T. Duong, S. L. Poojary, K. K. Dey, Y. Nishiyama and M. Ghosh, *J. Phys. Chem. C*, 2022, **126**, 17291–17305.
11 A. Hazari, M. R. Sawaya, N. Vlahakis, T. C. Johnstone, D. Boyer, J. Rodriguez, D. Eisenberg and J. A. Raskatov, *Chem. Sci.*, 2022, **13**, 8947–8952.
12 Y.-H. Huang, Q. Du, Z. Jiang, G. J. King, B. M. Collins, C. K. Wang and D. J. Craik, *Molecules*, 2021, **26**, 5554.
13 C. Zuo, W.-W. Shi, X.-X. Chen, M. Glatz, B. Riedl, I. Flamme, E. Pook, J. Wang, G.-M. Fang, D. Bierer and L. Liu, *Sci. China: Chem.*, 2019, **62**, 1371–1378.
14 A. Kai, B. D. Egleston, A. Tarzia, R. Clowes, M. E. Briggs, K. E. Jelfs, A. I. Cooper and R. L. Greenaway, *Adv. Funct. Mater.*, 2021, **31**, 2106116.
15 D. Wang, Y. Xin, D. Yao, X. Li, H. Ning, H. Zhang, Y. Wang, X. Ju, Z. He, Z. Yang, W. Fan, P. Li and Y. Zheng, *Adv. Funct. Mater.*, 2022, **32**, 2104162.
16 C. Ke, Z. Liu, S. Ruan, X. Feng and X. Liu, *Org. Chem. Front.*, 2021, **8**, 5705–5709.
17 J. Bernstein, *Polymorphism in Molecular Crystals*, Oxford University Press, Oxford, 2002, vol. 14.
18 S. Yang and G. M. Day, *J. Chem. Theory Comput.*, 2021, **17**, 1988–1999.
19 S. L. Price and S. M. Reutzel-Edens, *Drug Discovery Today*, 2016, **21**, 912–923.
20 S. L. Price, D. E. Braun and S. M. Reutzel-Edens, *Chem. Commun.*, 2016, **52**, 7065–7077.
21 J. T. Cross, N. A. Rossi, M. Serafin and K. A. Wheeler, *CrystEngComm*, 2014, **16**, 7251–7258.
22 S. L. Fomulu, M. S. Hendi, R. E. Davis and K. A. Wheeler, *Cryst. Growth Des.*, 2002, **2**, 645–651.
23 A. M. Lineberry, E. T. Benjamin, R. E. Davis, W. S. Kassel and K. A. Wheeler, *Crystal Growth Design*, 2008, **8**, 612–619.
24 J. M. Spaniol and K. A. Wheeler, *RSC Adv.*, 2016, **6**, 64921–64929.
25 F. Toda, K. Tanaka, H. Miyamoto, H. Koshima, I. Miyahara and K. Hirotsu, *J. Chem. Soc., Perkin Trans. 2*, 1997, 1877–1886.
26 A. K. Brandt, D. J. Boyle, J. P. Butler, A. R. Gillingham, S. E. Penner, J. M. Spaniol, A. K. Stockdill, M. M. Vanderwall, A. Yeraly, D. R. Schepens and K. A. Wheeler, *Crystals*, 2021, **11**, 1596.
27 A. Kumar, P. Singh and A. Nanda, *Appl. Microsc.*, 2020, **50**, 12.
28 I. C. Tinsley, J. M. Spaniol and K. A. Wheeler, *Chem. Commun.*, 2017, **53**, 4601–4604.
29 L. Kofler and A. Kofler, *Thermal micromethods for the study of organic compounds and their mixtures*, Wagner, Innsbruck, 1952.
30 W. C. McCrone, *Fusion Methods in Chemical Microscopy*, Wiley, New York, 1957.
31 M. C. Etter, J. C. MacDonald and J. Bernstein, *Acta Crystallogr., Sect. B: Struct. Sci.*, 1990, **46**, 256–262.
32 J. Bernstein, R. E. Davis, L. Shimoni and N.-L. Chang, *Angew. Chem., Int. Ed. Engl.*, 1995, **34**, 1555–1573.
33 C. F. Macrae, I. Sovago, S. J. Cottrell, P. T. A. Galek, P. McCabe, E. Pidcock, M. Platings, G. P. Shields, J. S. Stevens, M. Towler and P. A. Wood, *J. Appl. Cryst.*, 2020, **53**, 226–235.
34 C. R. Groom, I. J. Bruno, M. P. Lightfoot and S. C. Ward, *Acta Crystallogr., Sect. B: Struct. Sci., Cryst. Eng. Mater.*, 2016, **72**, 171–179.
35 P. R. Spackman, M. J. Turner, J. J. McKinnon, S. K. Wolff, D. J. Grimwood, D. Jayatilaka and M. A. Spackman, *J. Appl. Crystallogr.*, 2021, **54**, 1006–1011.
36 M. J. Frisch, *et al.*, *Gaussian 16 Rev. C.01*, 2016.
37 A. I. Kitaigorodski, *Molecular Crystals and Molecules*, Academic Press, New York, 1973.
38 Y. L. Slovokhotov, *Struct. Chem.*, 2019, **30**, 551–558.
39 S. Sirimulla, M. Lerma and W. C. Herndon, *J. Chem. Inf. Model.*, 2010, **50**, 194–204.